ISSN 1674-1056
http://cpb.iphy.ac.cn
http://iopscience.iop.org/cpb
中国物理 B
Chinese Physics
中国物理
Chinese Physics B

## Effects of Al component content on optoelectronic properties of $Al_xGa_{1-x}N$

Yan-Jun Ji(纪延俊), Jun-Ping Wang(王俊平), You-Wen Liu(刘友文)

**Citation:**Chin. Phys. B . 2018, 27(10): 106102. **doi:** 10.1088/1674-1056/27/10/106102

Journal homepage: http://cpb.iphy.ac.cn; http://iopscience.iop.org/cpb

**What follows is a list of articles you may be interested in**

---

### Studies on the nucleation of MBE grown III-nitride nanowires on Si

Yanxiong E(鄂炎雄), Zhibiao Hao(郝智彪), Jiadong Yu(余佳东), Chao Wu(吴超), Lai Wang(汪莱), Bing Xiong(熊兵), Jian Wang(王健), Yanjun Han(韩彦军), Changzheng Sun(孙长征), Yi Luo(罗毅)

Chin. Phys. B . 2017, 26(1): 016103. **doi:** 10.1088/1674-1056/26/1/016103

### Understanding of surface pit formation mechanism of GaN grown in MOCVD based on local thermodynamic equilibrium assumption

Zhi-Yuan Gao(高志远), Xiao-Wei Xue(薛晓玮), Jiang-Jiang Li(李江江), Xun Wang(王勋), Yan-Hui Xing(邢艳辉), Bi-Feng Cui(崔碧峰), De-Shu Zou(邹德恕)

Chin. Phys. B . 2016, 25(6): 066105. **doi:** 10.1088/1674-1056/25/6/066105

### Surface-type nonvolatile electric memory elements based on organic-on-organic CuPc-$H_2$Pc heterojunction

Khasan S. Karimov, Zubair Ahmad, Farid Touati, M. Mahroof-Tahir, M. Muqeet Rehman, S. Zameer Abbas

Chin. Phys. B . 2015, 24(11): 116102. **doi:** 10.1088/1674-1056/24/11/116102

### *In-situ* wafer bowing measurements of GaN grown on Si (111) substrate by reflectivity mapping in metal organic chemical vapor deposition system

Yang Yi-Bin, Liu Ming-Gang, Chen Wei-Jie, Han Xiao-Biao, Chen Jie, Lin Xiu-Qi, Lin Jia-Li, Luo Hui, Liao Qiang, Zang Wen-Jie, Chen Yin-Song, Qiu Yun-Ling, Wu Zhi-Sheng, Liu Yang, Zhang Bai-Jun

Chin. Phys. B . 2015, 24(9): 096103. **doi:** 10.1088/1674-1056/24/9/096103

### Influence of heavy ion irradiation on DC and gate-lag performance of AlGaN/GaN HEMTs

Lei Zhi-Feng, Guo Hong-Xia, Zeng Chang, Chen Hui, Wang Yuan-Sheng, Zhang Zhan-Gang

Chin. Phys. B . 2015, 24(5): 056103. **doi:** 10.1088/1674-1056/24/5/056103

---

# Effects of Al component content on optoelectronic properties of $Al_xGa_{1-x}N$*

Yan-Jun Ji(纪延俊)[1,2,†], Jun-Ping Wang(王俊平)[1,2], and You-Wen Liu(刘友文)[1,‡]

[1] College of Science, Nanjing University of Aeronautics and Astronautics, Nanjing 211106, China
[2] College of Aeronautical Engineering, Bingzhou University, Bingzhou 256603, China

(Received 19 June 2018; revised manuscript received 22 July 2018; published online 10 September 2018)

Using density functional theory, the electronic structures, lattice constants, formation energies, and optical properties of $Al_xGa_{1-x}N$ are determined with Al component content $x$ in a range from 0 to 1. As $x$ increases, the lattice constants decrease in e-exponential form, and the band gap increases with a band bending parameter $b = 0.3954$. The N–Al interaction force in the (0001) direction is greater than the N–Ga interaction force, while the N–Al interaction force is less than the N–Ga interaction force in the $(10\bar{1}0)$ direction. The formation energies under different Al component content are negative and increase with Al component content increasing. The static dielectric function decreases, the absorption edge has a blue shift, and the energy loss spectrum moves to high energy with the Al component content increasing.

**Keywords:** GaN, photocathode, electronic structure, optical properties

**PACS:** 61.72.uj, 71.22.+i, 61.80.Ba, 36.20.Kd **DOI:** 10.1088/1674-1056/27/10/106102

## 1. Introduction

For the less blind ultraviolet radiation source on Earth's surface, the solar blind ultraviolet (UV) detection for 200 nm∼280 nm holds the advantage of achieving all-round optical detection without dealing with background noise, and has important applications in astronomical observation, aerospace, missile early warning, and vacuum electronic source.[1,2] The III-nitride semiconductor GaN has attracted a great deal of attention in the past few years.[3–5] This is because it possesses important applications in light-emitting diodes (LEDs),[6,7] short-wavelength laser diodes (LDs),[8,9] UV detectors,[10,11] and solar cells.[12–14] The GaN-based photodetector can conveniently realize high-sensitivity visible-blind (McIntosh *et al.* 1999) and solar-blind (Tut *et al.* 2005) detections. GaN-based UV detectors have achieved extensive applications including missile detection and interception, biological and chemical agent detection, flame and environment monitoring, and UV astronomy, involving national defense, commerce, and scientific research. The ternary alloy $Al_xGa_{1-x}N$ is well tailored for covering a large region of the UV spectrum by changing the Al component content. By adjusting the Al component content, the optical band gap of ternary alloy $Al_xGa_{1-x}N$ can increase,[15,16] the optical absorption edge moves to the 280 nm blind ultraviolet band, and the sun-blind characteristic can completely be achieved. The responding wavelength of AlGaN is 239 nm–270 nm with the Al component content of 0.6–0.95,[17,18] while it is 280 nm for $Al_{0.5}Ga_{0.5}N/Al_{0.7}Ga_{0.3}N$,[19] and 280 nm–320 nm for PINI.[20]

The aim of this study is to examine the effect of the Al component content on the band gap and optical properties for wurtzite (WZ) $Al_xGa_{1-x}N$ films. An ordered 32-atom $Al_nGa_{16-n}N_{16}$ supercell, corresponding to the 2×2×2 conventional cells is used to model the $Al_xGa_{1-x}N$ alloy. The electronic band structure is obtained using first-principles calculations based on density functional theory (DFT) in the generalized gradient approximation (GGA). All calculations for the structures considered are performed with the CASTEP code.[21] Coulomb potential energy caused by electron–ion interaction is described using Vanderbilt's ultrasoft pseudopotentials,[22] in which the orbitals of Al ($3s^23p^1$), Ga ($3d^{10}4s^24p^1$), and N ($2s^22p^3$) are treated as valence electrons. A cutoff energy of 400 eV is used throughout the calculation of this study. The number of $k$ points used is 9×9×9 after making a series of tests and consulting the literature.

## 2. Electronic structure of GaN

The intrinsic GaN is a direct bandgap semiconductor with a band width of 3.39 eV[23] and an electron affinity of 4.1 eV[24] obtained experimentally. The band structure of GaN calculated in this article is shown in Fig. 1, where the dotted line indicates the Fermi level, the band gap is 1.66 eV consistent with the data obtained by Du *et al.*,[25] valence band top and conduction band bottom are at the $G$ point, the con-

*Project supported by the National Natural Science Foundation of China (Grant No. 61171042).
†Corresponding author. E-mail: jiyjun@126.com
‡Corresponding author. E-mail: youwen@163.com
© 2018 Chinese Physical Society and IOP Publishing Ltd 

duction band discontinuity is 1.76, while that of the Valence band is 0.71. There are three energy levels at the top of the valence band, they being the heavy hole zone, light hole zone, and split belt caused by coupling of spin orbit respectively. It can be seen from the total density of states (TDOS) (Fig. 2(a)) and partial density of states (PDOS) of Ga, N (Figs. 2(b) and 2(c)) atoms that the GaN valence band is mainly composed of Ga3d, N2s, and N2p state electrons, the conduction band is mainly composed of Ga4s and Ga4p state electrons, electrical transport properties of GaN and carrier type are mainly determined by N2p and Ga4s state electrons. Near the Fermi energy level, the bonds between Ga–N atoms are N2p with Ga4s, Ga4p, N2s with Ga4s, Ga4p in the conduction band, are N2p with Ga4s, Ga4p in the valence band, and are N2s with Ga3d in deep level.

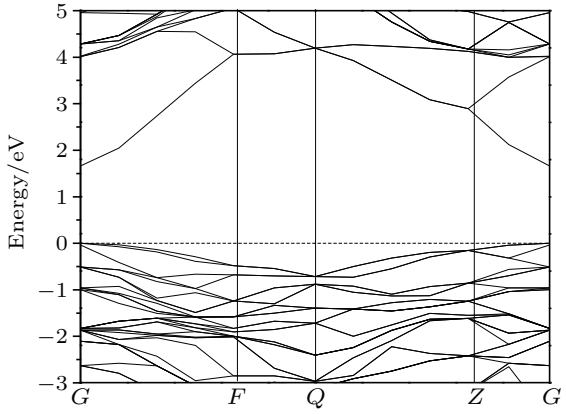



**Fig. 1.** Band structure of GaN.

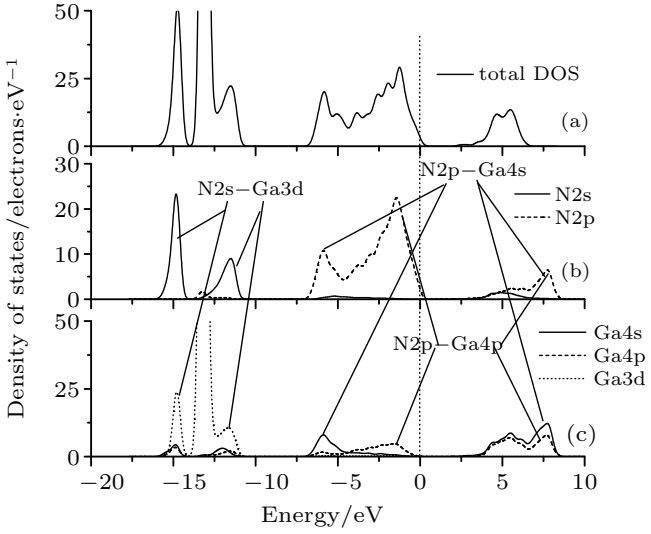



**Fig. 2.** (a) The total density of states of GaN, (b) partial density of states of N atoms, and (c) partial density of states of Ga atoms.

## 3. Electronic structure of $Al_xGa_{1-x}N$

The spectral response of GaN photocathode (see Fig. 3) was calculated by software COMSOL based on the finite element, the cutoff wavelength is about 370 nm, the peak wavelength is 310 nm in agreement with the test results calculated by Machuca *et al.*[20] In order to detect solar blind UV 280 nm, the Al component content must be adjusted to change the crystal band gap, and make the response wavelength blue shift.

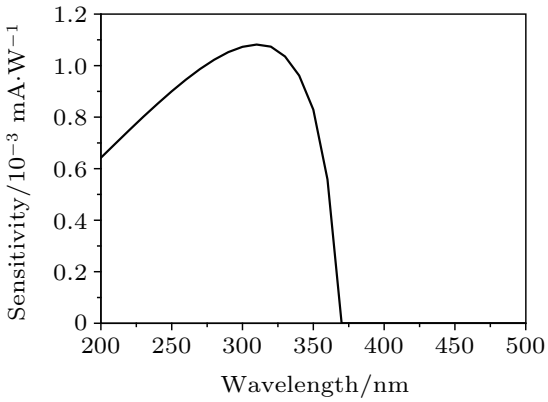



**Fig. 3.** Spectral response curve of GaN photocathode.

### 3.1. Crystal structure of $Al_xGa_{1-x}N$

Vegard's rule is the most extensive formula to describe $Al_xGa_{1-x}N$ lattice constants,[26] if the lattice constants for GaN (A1N) are $a$ and $c$, those of $Al_xGa_{1-x}N$ are expressed as

$$c(x) = c^{\mathrm{AlN}}(x) + c^{\mathrm{GaN}}(1-x), \tag{1}$$

$$a(x) = a^{\mathrm{AlN}}(x) + a^{\mathrm{GaN}}(1-x), \tag{2}$$

where the lattice constants for AlN (GaN) are $a = 3.112$ (3.189) Å, and $c = 4.982$ (5.185) Å. According to Vegard's rule, $a$ and $c$ have a linear relationship with $x$. The lattice constants for $Al_xGa_{1-x}N$ calculated (Table 1) in this article are fitted (Fig 4). According to linear fitting(line with stars), the lattice constant $a = 3.223 - 0.099x$ (Fig. 4(a)) with fitting degree 0.998, while $c = 5.285 - 0.243x$ (Fig. 4(b)) with fitting degree 0.997. According to e-exponential form (line with circles), the lattice constants can be expressed as $\alpha = \exp(1.17 - 0.034x + 0.00296x^2)$ (Fig. 4(a)), $c = \exp(1.658 - 0.038x - 0.008x^2)$ (Fig. 4(b)), the fitting degree is 0.999 for both $\alpha$ and $c$.

**Table 1.** Lattice constants of $Al_xGa_{1-x}N$.

| Al component | 0 | 0.125 | 0.25 | 0.375 | 0.5 | 0.625 | 0.75 | 0.875 | 1 |
|---|---|---|---|---|---|---|---|---|---|
| $a$/Å | 3.224 | 3.212 | 3.198 | 3.185 | 3.172 | 3.160 | 3.149 | 3.138 | 3.125 |
| $c$/Å | 5.253 | 5.226 | 5.199 | 5.170 | 5.140 | 5.110 | 5.078 | 5.042 | 5.009 |

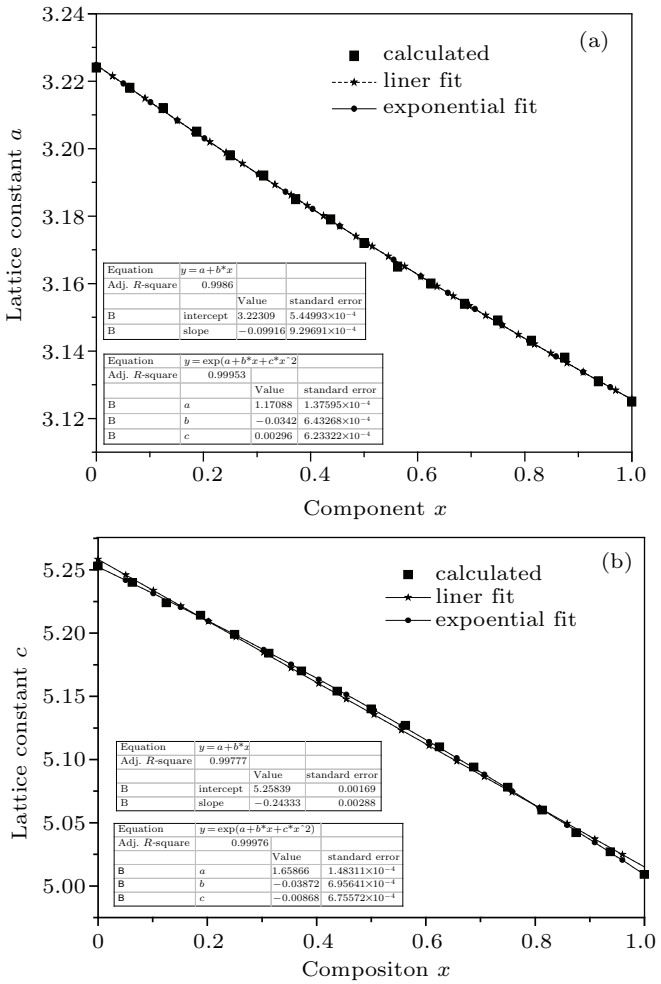



**Fig. 4.** Lattice constants (a) $a$ and (b) $c$ of $Al_xGa_{1-x}N$.

### 3.2. Densities of states and band structures of $Al_xGa_{1-x}N$

The densities of states (DOS) for $x$ from 0 to 1 are shown in Fig. 5. The valence band of $Al_xGa_{1-x}N$ is divided into two parts, they being the upper and lower valence bands. With the increase of Al component content, the energy distribution becomes narrower gradually and the peaks decrease in the conduction band and valence band. The lower valence band ranges from −15.89 eV to −10.72 eV, and its peak value decreases with Al component increasing. The separation zone of upper and lower valence bands is from −10.72 eV to −6.9 eV, and increases with Al component content increasing.

The upper valence band is in a range of −6.9 eV–0.44 eV energy, and becomes narrower gradually with Al composition increasing. This indicates that the effective electron mass increases with Al component content increasing. With the increase of Al component content, the range of valence band and conduct band become narrow, the reason is that the binding of the nucleus to the outer electrons of the Al atom is stronger than that of the Ga atom, for Ga atom has four shells, while Al atom has three shells.

Because the ion radius of $Al^{3+}$ (0.50 Å) is smaller than that of $Ga^{3+}$ (0.62 Å), and the electronegativity of $Al^{3+}$ (1.61) is less than that of $Ga^{3+}$ (1.81), $Al^{3+}$ will capture holes, and become the center of positive charge forming an isoelectronic trap, this will make the top of the conduction band move up gradually, the band gap increase gradually, and the charge number in the valence band increase with Al component content increasing.

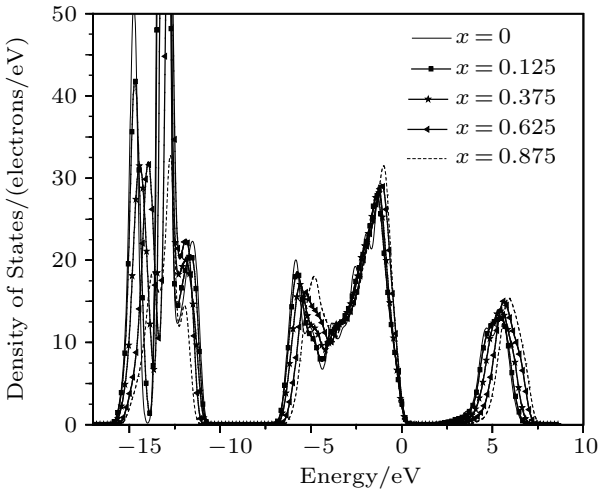



**Fig. 5.** Densities of states of $Al_xGa_{1-x}N$.

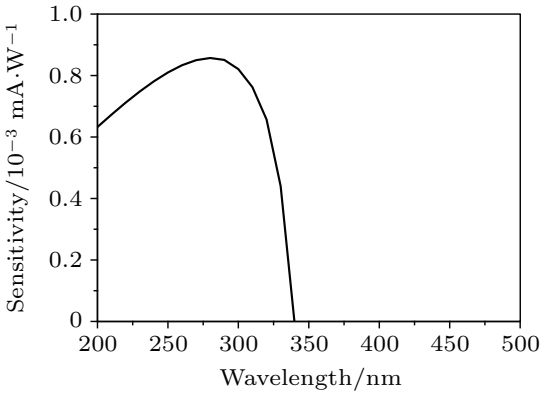



**Fig. 6.** Spectral response curve of $Al_{0.125}Ga_{0.875}N$.

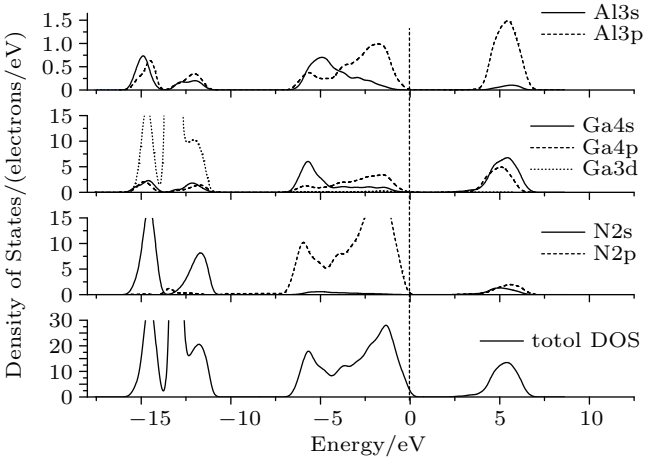



**Fig. 7.** Partial and total DOS of $Al_{0.125}Ga_{0.875}N$.

The spectral response of $Al_xGa_{1-x}N$ at $x = 0.125$ was calculated (see Fig. 6), the peak wavelength is 280 nm, which can satisfy the requirement for detecting the solar blind ultraviolet (UV). In order to study the electronic characteristics of solar blind ultraviolet detector material, the density of states of $Al_{0.125}Ga_{1-0.125}N$ was studied. The partial density of states (PDOS) with $x = 0.125$ is shown in Fig. 7. The valence electron of Al is $3s^2\ 3p^1$ in the calculation. The bonds between Al–N atoms are N2p with Al3s, N2s with Al3p in the conduction band, and that are N2p with Al3p, N2s with Al3s in the valence band. After Al composited, the span of Ga4s, Ga4p and N2s, N2p states is reduced in the conduction band, the DOS of N expands to the low energy in the valence band, while that of Ga expands to the high energy slightly, this indicates that the delocalization of electrons in high energy decreases, and the bonds of N2p with Ga4s, Ga4p, N2s with Ga4s Ga4p fade.

According to the experimental results of Angerer *et al.*, the band gap of $Al_xGa_{1-x}N$ is related to the composition of A1, and the relation links the width of the forbidden band to Al composition through the following equation[27]

$$E_g(x) = E_g^{GaN}(1-x) + E_g^{AlN}x - bx(1-x), \quad (3)$$

where $E_g(x)$ is the band gap energy of $Al_xGa_{1-x}N$, $E_g^{AlN}$ is the band gap energy of AlN, $E_g^{GaN}$ is the band gap energy of GaN, and $b$ is the band gap bowing parameter of $Al_xGa_{1-x}N$. The relationship between band gap and Al composition is calculated and fitted as shown in Fig. 8, it can be expressed as $E_g(x) = 0.3954x^2 + 1.988952x + 1.6815$. The fitting squared factor R is 0.99869. The physical origin of the band gap bowing can be attributed to the lattice mismatch between AlN and GaN. The larger mismatch in the lattice constants of the two binary alloys will result in the larger bowing. The experimental data of the band gap bowing parameter of WZ $Al_xGa_{1-x}N$ are divergent and are 0.69,[28] 0.74,[29] 1.0,[30,31] 1.3,[32,33] 1.38 eV,[34] and $1 \sim 0.67$ changing with strain,[35] the calculated value in this paper is $0.3954 \pm 0.0547$.

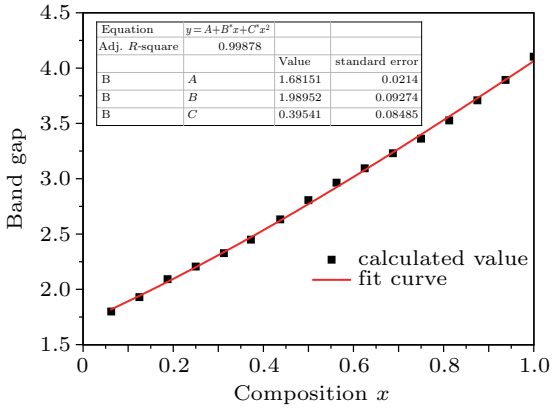



**Fig. 8.** (color online) Band gap of $Al_xGa_{1-x}N$.

### 3.3. Bonds of $Al_{0.125}Ga_{0.875}N$

In order to explain the atomic bonding clearly, the atomic overlap populations of the (0001) and $(10\bar{1}0)$ directions vertical to the (0001) direction are listed before and after Al has been composited for $x = 0.125$ in Table 2. For GaN, the overlap population is not the same in the (0001) direction as in the $(10\bar{1}0)$ direction, which indicates that the covalent bonds between Ga and N atoms are directional. Both in the (0001) direction and in the $(10\bar{1}0)$ direction, the covalent bonds between N atom and Ga atom are abated by being composited. The interaction between Al atom and N atom is stronger than that between Ga atom and N atom in the (0001) direction, and that between Al atom and N atom in the $(10\bar{1}0)$ direction. In the $(10\bar{1}0)$ direction, the interaction between Ga atom and N atom is stronger than that between Al atom and N atom.

**Table 2.** Overlap populations before and after being composited.

| Bond | Population Intrinsic | Composited |
|---|---|---|
| N–Ga/0001 surface | 0.58 | 0.50 |
| N–Ga/$10\bar{1}0$ surface | 0.66 | 0.64 |
| N–Al/0001 surface | | 0.63 |
| N–Al/$10\bar{1}0$ surface | | 0.59 |

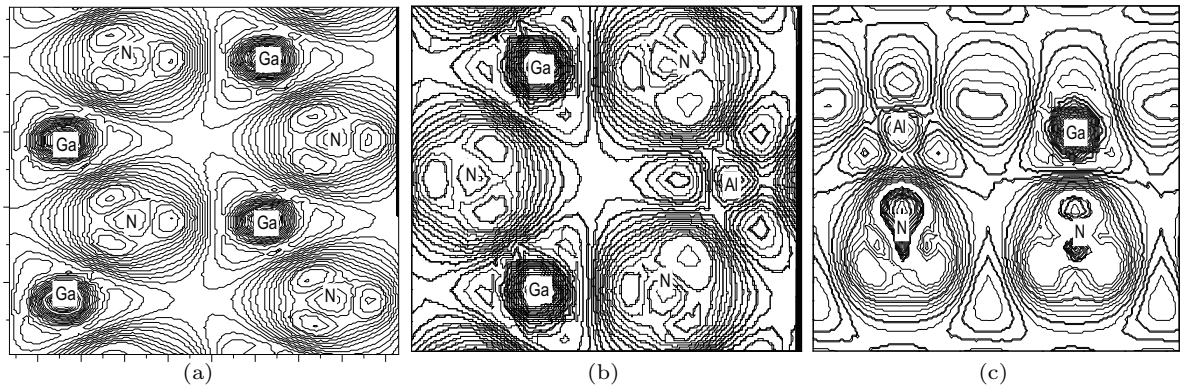



**Fig. 9.** Charge differential densities before and after Al composition: (a) uncomposited (0001), (b) composited (0001), and (c) composited $(10\bar{1}0)$.

The charge differential densities of $Al_{0.125}Ga_{0.875}N$ before (Fig. 9(a)) and after Al atoms have been composited for $x = 0.125$ in the (0001) direction (Fig. 9(b)) and the $(10\bar{1}0)$ direction (Fig. 9(c)) are calculated. For GaN, the electronic cloud around the N atom is distributed evenly with 3 Ga atoms in the (0001) plane. After Al atoms are composited, the electrons of the adjacent N atoms move towards the Al atoms, and the covalent bond between Al atom and N atom is stronger than that between Ga atom and N atom in the (0001) direction. Al composition makes the electrons of N atom adjacent to Al atom shift to Al atom, and the interaction between Ga atom and N atom weaker, so, the Ga 4s states move to a high energy, and the system band gap widens, the lattices and volume of the system become smaller.

### 3.4. Formation energy of $Al_xGa_{1-x}N$

After being optimized using the BFGS method, the formation energy of $Al_xGa_{1-x}N$ reasonable model can be expressed as[36]

$$E_{\text{form}} = -(E_{\text{tot}} + nE_{\text{N}} + mE_{\text{Ga}} + lE_{\text{Al}})/k, \tag{4}$$

where $E_{\text{tot}}$ is the total energy after being optimized, $n$, $m$, and $l$ are the number of N atoms, Ga atoms, and Al atoms, respectively, $k$ is the total number of atoms. The formation energies of $Al_xGa_{1-x}N$ with different Al component content are shown in Table 3.

The formation energies of $Al_xGa_{1-x}N$ with different Al component content are negative, which indicates that $Al_xGa_{1-x}N$ is a stable structure. With the increase of Al component content, the formation energies increase but the stability of the material decreases.

**Table 3.** Formation energies of $Al_xGa_{1-x}N$ with different Al component content.

| Al composition | 0 | 0.125 | 0.25 | 0.375 | 0.5 | 0.625 | 0.75 | 0.875 | 1 |
|---|---|---|---|---|---|---|---|---|---|
| Formation energy/eV | –133.2 | –133.0 | –32.9 | –132.7 | –132.5 | –132.3 | –132.2 | –132.0 | –131.8 |

## 4. Optical properties of $Al_xGa_{1-x}N$

The underestimation of the band gap results from the discontinuity of the exchange-correlation potential with respect to the particle number in first-principles calculations based on DFT, but accurate estimation of the valence band is a well-known consequence. To amend these band gaps, we calculate the optical properties by using scissors 1.73 eV with a rigid shift of the conduction band upwards with respect to the valence band from the known band gaps of GaN.

According to the definition of the direct transition probability and the Kramers–Kronig relation,[37] the optical properties parameters, such as the dielectric function, the light reflectance, the absorption coefficient, and the electrical conductivity can be deduced.

### 4.1. Dielectric function of $Al_xGa_{1-x}N$

Figure 10 shows the real part $\varepsilon_1(\omega)$ of the dielectric function of $Al_xGa_{1-x}N$ with different Al component contents. It can be seen that the material static dielectric function $\varepsilon_1(0)$ decreases with the increase of the Al component content. In the range of $\varepsilon_1(\omega) < 0$, the trough T1 moves to the high-energy range corresponding to the increase of the resonance frequency ($\omega_0$), while the trough T2 changes little corresponding to the little change of the plasma frequency ($\omega_p$) with the change of the Al component content.

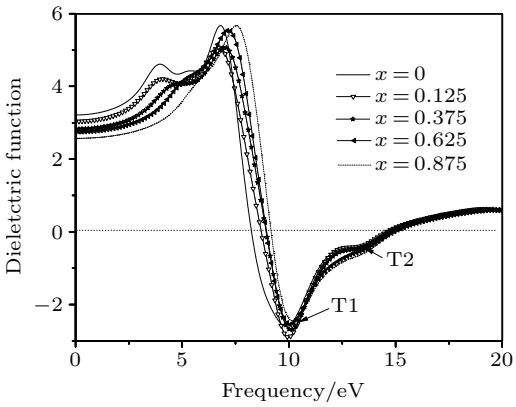



**Fig. 10.** Dielectric functions of $Al_xGa_{1-x}N$.

### 4.2. Absorption coefficient of $Al_xGa_{1-x}N$

The absorption coefficient curves of $Al_xGa_{1-x}N$ are shown in Fig. 11. With the increase of Al component content, the absorption edge moves to high energy, which is consistent with the phenomenon of the gap widening. With the increase of Al component content, the peak values decrease gradually until they disappear; the positions of peaks $P_3$ and $P_4$ do not change, but the peak values decrease. $P_1$ and $P_2$ correspond to the transition of Ga4s, Ga4p at the top of the valence band, and $P_4$ corresponds to the transition of the upper part of the lower valence band. The widening of the band gap makes the transition difficult and the absorption edge moves to high energy. The increase of $P_3$ indicates that N2p state electrons becomes more and more active with the increase of the Al component

content. The $P_2$ and $P_4$ decrease due to the fact that the activity of the Ga4s and Ga4p state electrons are more active than that of Al3s and Al3p.

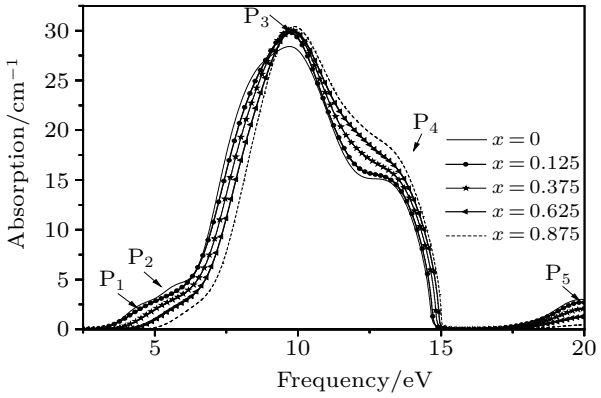



**Fig. 11.** Absorption coefficients of $Al_xGa_{1-x}N$.

### 4.3. Energy loss spectra of $Al_xGa_{1-x}N$

The energy loss spectra of $Al_xGa_{1-x}N$ are shown in Fig. 12, their peaks correspond to the material edge energy. With the increase of Al composition, the energy loss spectrum moves to high energy, which corresponds to the increase of the band gap.

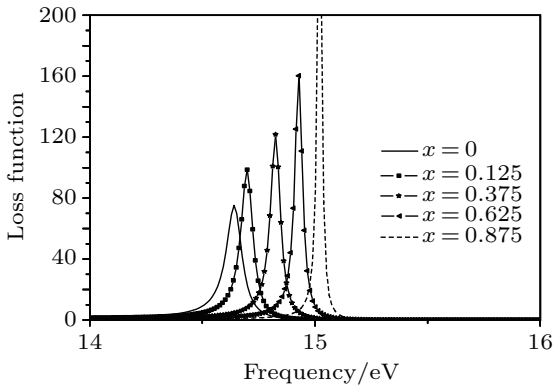



**Fig. 12.** Energy loss function of $Al_xGa_{1-x}N$.

## 5. Conclusions

The photoelectric characteristics of GaN are calculated by using the first principles, they being determined by N2p, N2s, Ga4s, and Ga4p states. The wavelength response peak of GaN is 310 nm. One Al atom replaces one Ga atom in order to obtain the ternary compound material $Al_xGa_{1-x}N$, its corresponding band being in the solar blind ultraviolet region. The wavelength response peak is 280 nm for $x = 0.125$. With the increase of Al composition, the lattice constants decrease, the band gap increases, the static dielectric function decreases, the absorption edge moves to high energy with peak value increasing. The Al composition changes the bonding between atoms, thus affecting the photoelectric characteristics of the system.

## References


[1] Shao J P, Han Y J, Wang L, Jiang Y, Xi G Y, Li H T, Zhao W and Luo Y 2006 *Chin. Phys. Lett.* **23** 432
[2] Zhang W, Xu J, Ye W, Li Y, Qi Z Q, Dai J N, Wu, Z H, Chen C Q, Yin J, Li J, Jiang H and Fang Y Y 2015 *Appl. Phys. Lett.* **106** 021112
[3] Isamu A and Hiroshi A 1997 *J. Appl. Phys.* **36** 5393
[4] Bar-Ilan A H, Zamir S, Katz O, Meyler B and Salzman 2001 *Mater. Sci. Eng. A* **302** 14
[5] Siegmund O H W, Tremsin A S, Vallerga J V, Mcphate J B and Hull J S 2008 *Proc. SPIE* **7021** 70211B
[6] Zhao H P, Liu G Y and Tansu N 2010 *Appl. Phys. Lett.* **97** 131114
[7] Chow W W 2011 *Opt. Express* **19** 21818
[8] Farrell R M, Hsu P S, Haeger D A, Fujito K, DenBaars S P, Speck J S and Nakamura S 2010 *Appl. Phys. Lett.* **96** 231113
[9] Zhang J, Zhao H P and Tansu N 2011 *Appl. Phys. Lett.* **98** 171111
[10] Dora Y, Arpan C, Lee M C, Stacia K, Stephen D B and Umesh M 2006 *IEEE Electron. Dev. L* **27** 713
[11] Wang X H, Chang B K, Ren L and Gao P 2011 *Appl. Phys. Lett.* **98** 1
[12] Bai, J, Gong, Y P, Li, Z and Wang T 2018 *Sol. Energy Mater. Sol. Cells* **175** 47
[13] Du X Q, Chang B K, Qian Y S and Pin G 2011 *Chin. Opt. Lett.* **9** 010401
[14] Liu, Sh M, Wang, Q, Xiao H L, Wang K, Wang C M, Wang X L, Ge W K and Wang Z G 2017 *Superlattices & Microstructures* **109** 194
[15] Ji Y J, Du Y J and Wang M S 2013 *Chin. Phys. B* **22** 117103
[16] Han D Y, Li H J, Zhao G J, Wei H Y, Yang S Y and Wang L S 2016 *Chin. Phys. B* **25** 048105
[17] Li X H, Xie H G, Ponce F A, Ryou J H and Detchprohm T 2015 *Appl. Phys. Lett.* **107** 241109
[18] Detchprohm T, Liu Y S, Mehta K, Wang S, Xie H G, Kao T T, Shen S C, Yoder P D, Ponce F A and Dupuis R 2017 *Appl. Phys. Lett.* **110** 011105
[19] Xie J, Mita S, Bryan Z, Guo W and Hussey L 2013 *Appl. Phys. Lett.* **102** 171102
[20] Yao Ch J, Ye X C and Sun R 2017 *Appl. Phys. A* **123** 439
[21] Milman V, Winkler B, White J A, Pickard C J, Payne M C, Akhmatskaya E V and Nobes R H 2000 *J. Quantum Chem.* **77** 895
[22] Vanderbilt D 1990 *Phys. Rev. B* **41** 7892
[23] Dmitriev A V, Oruzheinikov A L, eds. Gaskill D K, Brandt C D and Nemanich R J 1996 *Material Research Society Symposium Proceedings*, Pittsburgh PA **423** 69
[24] Bougrov V, Levinshtein M E, Rumyantsev S L, Zubrilov A 2001 eds. Levinshtein M E, Rumyantsev S L and Shur M S (New York: John Wiley & Sons, Inc.) p. 1
[25] Du Y J, Chang B K, Zhang J J, Wang X H, Li B and Wang M S 2011 *Adv. Mater. Rapid Commun.* **5** 1050
[26] Vegard L 1921 *Z. F. Phys.* **5** 17
[27] Angerer H, Brunner D, FreudenbeRg F, Ambacher O, Stutzmann M, Hopier R, Metzger T, Bom E, Dollinger G, Bergmaier A, Karsch S and Komer H J 1997 *Appl. Phys. Lett.* **71** 1504
[28] Lee S R, Wright A F, Crawford M H, Petersen G A, Han J and Biefeld R M 1999 *Appl. Phys. Lett.* **74** 3344
[29] Roberto N G, Armando R S, Alvaro P A and Donald H G 2008 *Rev. Mex. Fis.* **54** 111
[30] Yun F, Reshchikov M A, He L, King T, Morkoç H, Novak S W and Wei L 2002 *J. Appl. Phys.* **92** 4837
[31] Nepal N, Li J, Nakarmi M L, Lin J Y and Jiang H X 2005 *Appl. Phys. Lett.* **7** 242104
[32] Brunner D, Angerer H, Bustarret E, Freudenberg F, Hopler R, Dimitrov R, Ambacher O and Stutzmann M 1997 *J. Appl. Phys.* **82** 5090
[33] Shan W, Ager III J W, Yu K M and Walukiewicz W 1999 *J. Appl. Phys.* **85** 8505
[34] Katz, O, Meyler B, Tisch U, Salzman J 2001 *Phys. Status Solidi (A) Appl. Res.* **188** 789
[35] Liou B T, Kuo Y K 2012 *Appl. Phys. A* **106** 1013
[36] Yu X H, Du Y J, Chang B K, Ge Z H and Wang H G 2013 *Optik* **124** 4402
[37] Lucarini V, Sarrinen J J, Peiponen K E and Vartiainen E M 2005 *Kramers–Kronig Springer Series in Optical Seciences* (Berlin/Heidelberg/New York: Springer)